Reports

Length-of-Day Variations Caused by El Niño–Southern Oscillation and Quasi-Biennial Oscillation

B. FONG CHAO

Two prominent interannual atmospheric fluctuations, the El Niño–Southern Oscillation in the troposphere-ocean system and the Quasi-Biennial Oscillation in the equatorial stratosphere, account for most of the observed interannual length-of-day (LOD) variation from 1964 through 1987, with a relative contribution of about 2 to 1. Thus the atmosphere-LOD connection extends from seasonal and shorter periods to interannual periods up to about 10 years.

TO CONSERVE TOTAL ANGULAR MOMENTUM, any motion and redistribution of material inside or on the surface of the earth is accompanied by variations in the solid earth's rotation. Knowledge of this momentum exchange is fundamental in understanding the earth system dynamics. In this report, I focus on the excitation of interannual variations in the earth's axial spin, or equivalently the length-of-day (LOD) variations, caused by two prominent interannual fluctuations in the atmosphere, the El Niño–Southern Oscillation (ENSO) and the Quasi-Biennial Oscillation (QBO). Post-glacial rebound, core-mantle interactions, and tidal dissipation are believed to cause the long-term (decade to secular) variations in LOD (*1*). On the other hand, seasonal and shorter period LOD changes have been clearly linked to atmospheric angular momentum variations (*2*).

The most prominent interannual fluctuation in the troposphere-ocean system, ENSO is characterized by an irregular seesawing of air mass between the Eastern and Western hemispheres in the tropical and subtropical Pacific-Indian ocean region (*3*). During an El Niño, the normal tropical easterly wind field collapses, causing extensive meteorological disruptions that last 14 to 18 months. The QBO, the dominant phenomenon in the equatorial stratosphere, is a regular alternation in the mean zonal wind and temperature regimes, with a period varying from 24 to 30 months (*4, 5*).

Several studies have shown that ENSO has a significant influence on the interannual LOD variation (*6, 7*). Chao (*7*), however, reported that ENSO and LOD correlated poorly at biennial periods and hence speculated that QBO might also influence LOD. In this report, using data for the period of 1964 through 1987, I investigate the combined effect of ENSO and QBO on interannual LOD variations with correlation studies.

Geodynamics Branch, Goddard Space Flight Center, Greenbelt, MD 20771.

Interannual signals were first extracted from LOD, ENSO, and QBO data sets. The LOD variation data were obtained through a three-point differentiation of a homogeneous data set of universal time at 5-day intervals (*8*). To enable the comparison of the 5-day LOD time series with monthly meteorological series, I converted the LOD series to monthly series by linear interpolation and decimation, but only after the series had been smoothed with a moderate low-pass filter. The least-squares fit of a combination of annual and semiannual sinusoids as well as a third-degree polynomial were then subtracted from the LOD series. The polynomial was used to remove the mean, the linear trend, and decade-scale curvature from the time series, so that the remaining interannual variation has periods from 1 to about 10 years. The peak-to-peak amplitude is ~0.5 ms.

Ideally, the axial angular momentum of ENSO (and hence its influence on LOD) should be obtained from a global integration of atmospheric (and possibly oceanic) data. However, this approach does not separate the angular momentum attributable to ENSO from that of non-ENSO origin. Therefore, adopting the approach of Chao (*7*), I used a proxy representation of ENSO similar to the standard Southern Oscillation Index (*3*). Specifically, the difference $P_T(t) - P_D(t)$ for 1964 to 1987 was constructed, where $P_T(t)$ and $P_D(t)$ denote the monthly sea-level barometric pressure series at Tahiti and Darwin, Australia. The interannual variations in $P_T(t)$ and $P_D(t)$ are highly and negatively correlated because the two stations are located near opposite poles of the ENSO pressure seesaw (*3*). The $P_T(t) - P_D(t)$ series was then passed through the low-pass filter, and a mean and the seasonal signals were subsequently removed as for LOD.

The axial angular momentum associated with the alternating zonal wind of QBO was estimated from monthly averages of zonal wind speed, u, recorded at three selected stations each at three pressure levels (*9*). The stations are Singapore (1.3°N, 104°E), Balboa (in Panama, 9°N, 80°W), and Ascension Island (8°S, 15°W). The pressure levels are 50 mb (corresponding to an altitude of about 20.7 km), 30 mb (23.7 km), and 10 mb (31.3 km). I established the complete QBO wind field by extrapolating and interpolating the data with the following assumptions (*4, 5, 9*): (i) the volume V within which QBO is confined is a torus around the globe above the equator that has a fan-shaped cross section delimited in latitude between ±30° and in altitude in terms of pressure between 105 mb (15.7 km) and 5 mb (35.4 km); (ii) u is independent of longitude; (iii) at any given altitude, the phase of u is independent of latitude; (iv) the phase of u propagates downward in altitude at the rate of 1 km per month; (v) at any latitude, the amplitude profile of u along altitude follows that of Wallace (*4*), with a maximum at 30 mb level; and (vi) the amplitude of u averaged over altitude is highest at the equator and tapers off symmetrically toward higher latitudes accord-

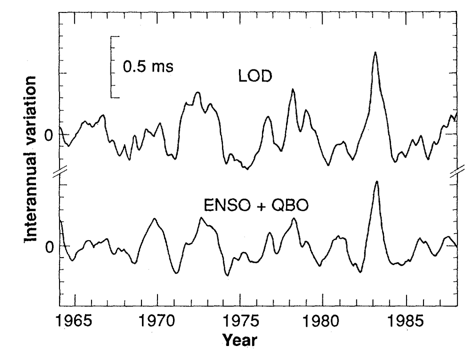

Fig. 1. Comparison of the interannual LOD variation $[L(t)]$ with the least-squares fit of a linear combination of ENSO and QBO variations $[eE(t) + qQ(t)]$ from 1964 to 1987. The 2-month phase shift in $E(t)$ and the 1-month shift in $Q(t)$ (see text) are included.

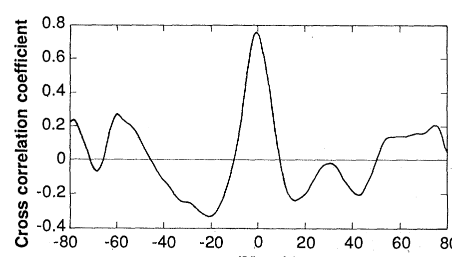

Fig. 2. The cross correlation between the two time series in Fig. 1 (the interannual LOD variation with the least-squares combination of ENSO and QBO variations), as a function of phase lag τ between −80 to 80 months. The correlation coefficient (at zero lag) is 0.75.

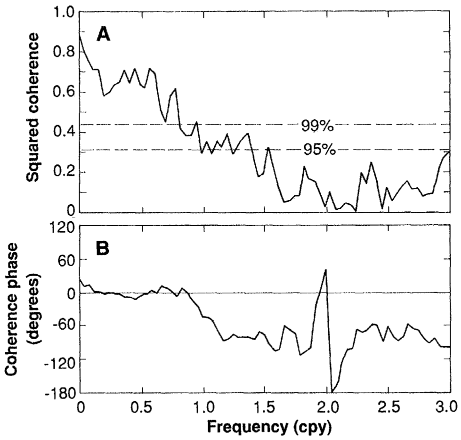

Fig. 3. The squared coherence (**A**) and coherence phase spectra (**B**) between the two time series in Fig. 1 (the interannual LOD variation with the least-squares combination of ENSO and QBO variations) (*12*). The 99% and 95% confidence thresholds for the squared coherence are indicated by dashed horizontal lines.

ing to $(1 + \cos 6\theta)/2$, where θ is the latitude. Furthermore, I assume that the pressure along the altitude is in hydrostatic equilibrium with an average scale height of 6.47 km and a nominal (constant) temperature of 240 K in V. The QBO angular momentum is then computed by integration over V. The mean value as well as any seasonal signals that may be present were removed by the subtraction of the mean monthly values. The QBO seasonal signal (that has been removed) is relatively small in amplitude, corresponding only to a total LOD variation of about 0.012 ms, whereas the QBO interannual component has a peak-to-peak amplitude of about 0.2 ms (*10*).

The time series derived above for ENSO and QBO variations were processed further to facilitate comparisons: the ENSO series was shifted forward in time by 2 months and the QBO series by 1 month. The 2-month shift in the ENSO series relative to LOD is justified because it produces the maximum correlation between them (*7*). The 1-month shift of QBO is less clear; numerically it results in a slightly better correlation with LOD (see below) than without it. Superficially, this shift suggests that the QBO influence takes a month to be transmitted to the solid earth (*11*). However, in consideration of assumption (iv) above and in that 1 month is the resolving interval of the time series, this shift is only nominal and its physical significance is uncertain.

The relation among the final time series, denoted $L(t)$ (for LOD in units of milliseconds), $E(t)$ (for ENSO in millibars), and $Q(t)$ (for QBO in equivalent milliseconds), can be investigated in the form

$$L(t) \simeq eE(t) + qQ(t) \qquad (1)$$

The coefficient e gives the LOD change per unit change of $E(t)$, whereas q is dimensionless. They are free parameters to be determined in some optimal fashion. A least-squares fit performed on Eq. 1 gives $e = -0.0813$ ms mb^{-1} and $q = 0.941$. A comparison of $L(t)$ with $[eE(t) + qQ(t)]$ shows good agreement (Figs. 1 and 2).

The misfit arises from measurement noise, modeling errors (such as nonlinearity in the ENSO-LOD relation), as well as other unaccounted LOD excitation sources on the interannual time scale under consideration. Ideally, if ENSO and QBO constitute the total interannual LOD excitation, as implied in Eq. 1, then the misfit should be small in magnitude. More importantly, under the conservation of angular momentum, the coefficient q should be unity if, in addition, the QBO angular-momentum estimate is sufficiently accurate and QBO is linearly uncorrelated with ENSO. Our estimate of q is indeed close to 1 (within about 6%), indicating that the above assertions are valid. The estimate of e is such that, for example, the drop of about 7 mb in $E(t)$ during the strong 1982–1983 El Niño episode corresponds to a 0.57-ms lengthening in LOD or an increase of 3.4×10^{25} kg m^2 s^{-1} in atmospheric angular momentum, in good agreement with observations (*6*).

The standard deviations of the two terms on the right side of Eq. 1 are 0.124 ms for $eE(t)$ and 0.064 ms for $qQ(t)$. Thus ENSO and QBO contribute to the interannual LOD excitation at the ratio of about 2 to 1.

For a spectral break down of the overall cross correlation (Fig. 2), the complex coherence spectrum between $L(t)$ and $[eE(t) + qQ(t)]$ was computed (Fig. 3) (*12*). The squared coherence spectrum, for a spectral averaging length of nine elementary widths, can be judged against the corresponding confidence threshold (*13*): 0.31 for 95% confidence and 0.44 for 99% confidence. High coherence indeed concentrates in the interannual frequency range; the values are above the 95% threshold for up to about 1.4 cpy (cycles per year). More strikingly, the coherence values around biennial periods (~0.5 cpy) are well in excess of the 99% threshold, in contrast to the poor coherence at biennial periods found between LOD and ENSO alone by Chao (*7*). This coherence is a clear manifestation of the strong influence of QBO on LOD at biennial periods.

The coherence phase spectrum (Fig. 3) shows a near-zero phase throughout the interannual frequency range, which is further confirmation of the correlation between ENSO + QBO and LOD. This result also substantiates the time shifts that were made in $E(t)$ and $Q(t)$ relative to $L(t)$ in order to acquire maximum correlation (described above).

Finally, in order to illustrate the correlation of LOD with QBO alone, $qQ(t)$ is compared with the low-passed difference of $L(t)$ and $eE(t)$, $[L(t) - eE(t)]$. Normally this difference is not desirable because the differencing of two highly correlated time series greatly amplifies the relative noise level in the residual series. Despite this effect, the general agreement in both magnitude and phase (Fig. 4) is striking. The cross-correlation function between them oscillates with a periodicity of ~29 months (common in both series), with a correlation coefficient of 0.48.

Correlation studies thus indicate that ENSO and QBO, with relative contribution of about 2 to 1, can account for most, if not all, of the observed interannual LOD variations. Seasonal and shorter period LOD variations are known to have their origin in the atmosphere; these results indicate that the atmosphere-LOD connection extends to the interannual period range from [illegible] to 10 years.

Fig. 4. Comparison of QBO variation, $[qQ(t)$ (solid curve)], with the smoothed difference between interannual LOD and ENSO variations $[L(t) - eE(t)$ (dashed curve)] from 1964 to 1987.

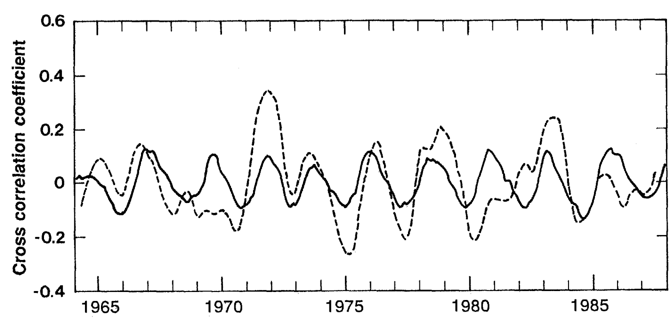

REFERENCES AND NOTES

1. For a review, see K. Lambeck, *The Earth's Variable Rotation* (Cambridge Univ. Press, New York, 1980).
2. R. D. Rosen and D. A. Salstein, *J. Geophys. Res.* **88**, 5451 (1983).
3. For a review, see E. M. Rasmusson and T. H. Carpenter, *Mon. Weather Rev.* **110**, 354 (1982); E. M. Rasmusson, *Am. Sci.* 73, 168, (1985).
4. J. M. Wallace, *Rev. Geophys. Space Phys.* **11**, 191 (1973).
5. R. A. Plumb, in *Dynamics of the Middle Stratosphere*, J. R. Holton and T. Matsuno, Eds. (Reidel, Boston, 1984), pp. 217–251.
6. R. D. Rosen, D. A. Salstein, T. M. Eubanks, J. O. Dickey, J. A. Steppe, *Science* **225**, 411 (1984); D. A. Salstein and R. D. Rosen, *J. Clim. Appl. Meteorol.* **25**, 1870 (1986); B. F. Chao, *Geophys. Res. Lett.*

11, 541 (1984).
7. B. F. Chao, *J. Geophys. Res.* **93**, 7709 (1988).
8. The data are based on measurements published by BIH (Bureau International de l'Heure, Paris) together with those obtained by LAGEOS satellite laser ranging; see E. C. Pavlis, M. H. Torrence, R. Kolenkiewicz, *Eos* **68**, 1245 (1987).
9. J. K. Angell, *Mon. Weather Rev.* **114**, 2272 (1986).
10. Angular momentum is converted to equivalent LOD with the conversion factor of 0.0168 ms per 10^{24} kg m^2 s^{-1} (Fig. 4).
11. Indications of a link between the stratospheric QBO and a tropospheric QBO in the Southern Hemisphere was reported by K. E. Trenberth [*Mon. Weather Rev.* **108**, 1370 (1980)].
12. Figure 3 shows only the frequency range from 0 to 3 cpy; spectral values at higher frequencies (up to the Nyquist frequency of 6 cpy) may not be realistic because spectral energy decreases rapidly with increasing frequency, especially after the data have been low-pass filtered.
13. For example, P. Bloomfield, *Fourier Analysis of Time Series: An Introduction* (Wiley, New York, 1976).
14. I thank J. K. Angell, V. Kousky, and E. Pavlis for providing the data used in this study. I particularly thank K. S. Chiu for his assistance in data preparation and computation. A more complete description of the analysis is in B. F. Chao, *NASA–Goddard Space Flight Center Lab. Terrest. Phys. Prof. Publ.* (1988).

3 October 1988; accepted 23 December 1988

Cordierite-Spinel Troctolite, a New Magnesium-Rich Lithology from the Lunar Highlands

URSULA B. MARVIN, J. WILLIAM CAREY, MARILYN M. LINDSTROM

A clast of spinel troctolite containing 8 percent cordierite ($Mg_2Al_4Si_5O_{18}$) has been identified among the constituents of Apollo 15 regolith breccia 15295. The cordierite and associated anorthite, forsteritic olivine, and pleonaste spinel represent a new, Mg-rich lunar highlands lithology that formed by metamorphism of an igneous spinel cumulate. The cordierite-forsterite pair in the assemblage is stable at a maximum pressure of 2.5 kilobars, equivalent to a depth of 50 kilometers, or 10 kilometers above the lunar crust-mantle boundary. The occurrence of the clast indicates that spinel cumulates are a more important constituent of the lower lunar crust than has been recognized. The rarity of cordierite-spinel troctolite among lunar rock samples suggests that it is excavated only by large impact events, such as the one that formed the adjacent Imbrium Basin.

RARE SPINEL-BEARING TROCTOLITES and cataclasites among lunar highland samples have provided evidence that spinel cumulate layers occur near or below the lunar crust-mantle boundary. A small white clast of spinel troctolite containing crystals of red spinel and grains of cordierite up to 0.3 mm long (Fig. 1, A and B) was found during an investigation of Apollo 15 regolith breccias. Electron microprobe analyses (Table 1) show that this mineral is essentially pure magnesium-cordierite, with <1 weight percent of FeO and no evidence of H_2O, which generally equals 0.5 to 3.0 weight percent in terrestrial cordierites. The troctolite is composed of 75% plagioclase (anorthite), 11% olivine (forsterite), 8% cordierite, 6% spinel (pleonaste) and <0.5% accessory minerals (Table 2). The accessories include small, sparse grains of magnesium-ilmenite, rutile, troilite, metal, and two minute particles of a calcium-phosphorous–bearing phase (apatite?) that are too small for quantitative analyses. The Ni and Co concentrations ($\leq Ni_{55}Co_{3.7}$) in the metal grains (Table 2) are markedly higher than those that have been measured in metals of either meteoritic or lunar provenance from most lunar rocks and soils, but they are comparable with concentrations reported in metals of certain spinel-bearing lunar rocks of deep-seated origin, including spinel troctolite 67435 (*1*) and dunite 72415 (*2*). The calculated bulk composition shows that the cordierite-spinel troctolite is corundum- and nepheline-normative (Table 3).

The small clast of cordierite-spinel troctolite in sample 15295,101 has a well-crystallized mineral assemblage that has undergone minor in situ cataclasis. Anorthite (An_{93}) occurs in coarse-grained, twinned fragments, <0.9 mm long, that are bordered, in some instances, by finely crushed material of the same composition. Cordierite occurs in equant grains, one of which displays the hexagonal sector twinning characteristic of the mineral (Fig. 1C), and in anhedral grains between other mineral pairs (Fig. 1D). The spinel and olivine also occur in two habits: as large euhedral to subhedral crystals, and as small grains aligned along grain boundaries in the clast and between the clast and breccia matrix. Pleonaste is present as euhedral grains up to 0.25 mm in diameter and also in rows of tiny <0.01-mm crystals (Fig. 1D). Some of the larger pleonaste crystals are lustrous and smooth whereas others have pitted surfaces, suggestive of alteration. However, all of the pleonaste grains, large and small, are unzoned and similar in composition. Forsterite (Fo_{90} to Fo_{92}) occurs in subhedral grains (<0.15 mm) with an optically patchy mosaic texture and in thin stringers along grain boundaries (Fig. 1D). The composition is essentially uniform within grains and from grain to grain.

The significance of the textural relations is uncertain. We believe, for reasons discussed below, that this cordierite-spinel troctolite is a metamorphic assemblage. Two generations of olivine, spinel, and cordierite (ol-sp-crd) grains may be present, consisting of large crystals that formed early, and small, interstitial ones that formed later. Alternatively, the growth patterns may reflect an increasing geometric confinement of the modally subordinate ol-sp-crd assemblage to edges and interstices of the plagioclase grains during a single, extended period of crystallization.

Spinel-bearing troctolites and cataclasites are among the rarer rock types in lunar highland samples. The spinel troctolites

Table 1. Bulk rock and mineral compositions of the cordierite-spinel troctolite clast in weight percent.

Component	Bulk* rock	Cordierite (20)†	Spinel (18)†	Olivine (24)†	Plagioclase (20)†
SiO_2	38.58	50.85	0.02	40.30	45.08
Al_2O_3	29.85	34.26	56.61	0.05	34.34
FeO	3.15	0.84	9.97	8.72	0.02
MgO	13.79	13.34	20.47	50.65	0.05
CaO	12.25	0.05	0.05	0.06	19.34
Na_2O	0.41	0.03	0.00	0.00	0.65
K_2O	0.09	0.49	0.00	0.00	0.12
TiO_2	0.06	0.06	0.11	0.05	0.05
Cr_2O_3	1.62	0.02	12.73	0.03	0.02
MnO	0.03	0.02	0.05	0.10	0.01
P_2O_5	0.17	0.02	0.00	0.03	0.26
Total	100.00	99.98	100.01	99.99	99.94

*Bulk composition calculated from mode (Table 2) and assigning all Fe to FeO. †Numbers in parentheses give number of points analyzed and averaged from six or more grains of each mineral.

U. B. Marvin, Harvard–Smithsonian Center for Astrophysics, Cambridge, MA 02138.
J. W. Carey, Department of Earth and Planetary Sciences, Harvard University, Cambridge, MA 02138.
M. M. Lindstrom, National Aeronautics and Space Administration, Johnson Space Center, Houston, TX 77058.